

Relativistic mean-field study of light nuclei near drip line

B. K. Agrawal¹, Tapas Sil¹, S. K. Samaddar¹ and J. N. De²

¹Saha Institute of Nuclear Physics, 1/AF Bidhannagar, Calcutta 700 064, India

²Variable Energy Cyclotron Centre, 1/AF Bidhannagar, Calcutta 700 064, India

Abstract

The relativistic mean field theory is applied to study some exotic properties of neutron rich nuclei as recently observed, namely, extension of the drip-line for F nuclei from ^{29}F to ^{31}F and the appearance of a new shell closure at neutron number $N = 16$. We find ^{31}F to be bound against one-neutron dripping but unbound only marginally for two neutron separation. The calculated functional dependence of one-neutron separation energy with neutron number for different values of $T_Z = (N - Z)/2$ signals a new shell closure at $N = 16$ for neutron rich nuclei with $T_Z \geq 3$. This is further corroborated from the study of the deformation and the gap across the Fermi surface in these light nuclei.

PACS Number(s): 21.60.-n, 21.30.Fe, 27.30+t

Keywords: Relativistic mean-field, drip line, shell closure

I. INTRODUCTION

Recent experiments with radioactive ion beams have mapped out neutron drip line nuclei around $N = 20$ and $N = 28$ [1,2]. These exotic nuclei with high isospins have many peculiar properties quite distinct from those found in the stability valley. The usual shell closures at $N = 20$ and 28 have been questioned, new shell closures have been predicted and doubts have been expressed for the validity in this region of the usual nucleon-nucleon interaction or nuclear matrix elements which are so successful in describing the nuclei close to the stability line. The neutron-rich nuclei near the drip line show large neutron skin or neutron halo and the radii are larger than those expected from the usual $r_0 A^{1/3}$ law. A number of "Borromean" nuclear systems like ^{11}Li , ^{31}F , ^{32}Ne etc. have been discovered which result in unstable nuclei after one neutron removal but stable ones on two neutron removal. These are only a few of the exotic properties found in nuclei near the drip line.

There have been a number of attempts, both in the non-relativistic as well as in the relativistic frameworks, to understand the properties of nuclei in the vicinity of the drip line. In different models, though some of the properties are qualitatively the same, there are also some striking differences. As for example, experimental results [3] show that ^{32}Mg is highly deformed ($\beta_2 \sim 0.5$) whereas the RMF theory predicts [4] nearly spherical configuration for this isotope; the shell model calculations with relatively smaller model space also have similar conclusions [5]. On the other hand, a recent shell model calculation carried out in the extended model space [6] produce deformation in consonance with the experimental finding. However, some anomalies persist in the binding energies of some nuclei around the drip line.

Several calculations of drip line nuclei around $N = 28$ have been performed applying the RMF theory in the Hartree-BCS [7] as well as within the Hartree-Bogoliubov [8] framework. The coordinate space description of the RMF theory in the spherical configuration has been used [9] for the study of neutron rich nuclei

around $N = 20$. With the advancement of radioactive ion beam techniques, the neutron drip line is getting shifted to higher N -value. As for example, a recent experiment at RIKEN [2] shows that ^{31}F rather than ^{29}F is the most likely candidate for the drip line fluorine isotope. It is conjectured [2] that onset of deformation is responsible for the extrastability for ^{31}F .

Recent analyses [10] of the single-neutron separation energies S_n and other experimental data for neutron-rich light nuclei, however, indicate the appearance of a new magic number at $N=16$ and the disappearance of the traditional magicity at $N=20$. Dissolution of the $N=8$ magic number in neutron-rich *Li* and *Be* isotopes [11,12] and the appearance of magicity at $N=6$ in 8He [13] have also been pointed out. The structures of these nuclei near the drip line are discussed in reference to the picture of the island of inversion [14] and have recently been systematically studied in the framework of Monte-Carlo shell model (MCSM) [15,6]. In the present work, we will focus on the theoretical understanding of the extension of the drip line in *F* chain and the appearance of shell closure at $N=16$ in the light of relativistic mean field framework.

The organization of the paper is as follows. In Sec. II, the formalism used have been out-lined very briefly. In Sec. III, the results and discussions are given. Finally, in Sec. IV, we present the summary and the concluding remarks.

II. FORMALISM

The details of the formalism of the RMF theory for calculating various observables like deformation, total energy etc. can be found in Refs. [16,17]. However, for the sake of completeness we write down the effective Lagrangian density used describing the nucleon-meson many-body systems followed by a brief discussion. The Lagrangian density reads

$$\mathcal{L} = \bar{\Psi}_i (i\gamma^\mu \partial_\mu - M) \Psi_i + \frac{1}{2} \partial^\mu \sigma \partial_\mu \sigma - U(\sigma) - g_\sigma \bar{\Psi}_i \sigma \Psi_i$$

$$\begin{aligned}
& -\frac{1}{4}\Omega^{\mu\nu}\Omega_{\mu\nu} + \frac{1}{2}m_\omega^2\omega^\mu\omega_\mu - g_\omega\bar{\Psi}_i\gamma^\mu\omega_\mu\Psi_i - \frac{1}{4}\vec{R}^{\mu\nu}\vec{R}_{\mu\nu} + \frac{1}{2}m_\rho^2\vec{\rho}^\mu\vec{\rho}_\mu \\
& - g_\rho\bar{\Psi}_i\gamma^\mu\vec{\rho}_\mu\vec{\tau}\Psi_i - \frac{1}{4}F^{\mu\nu}F_{\mu\nu} - e\bar{\Psi}_i\gamma^\mu\frac{(1-\tau_3)}{2}A_\mu\Psi_i.
\end{aligned} \tag{1}$$

The scalar-isoscalar meson σ , the vector-isoscalar meson ω and vector-isovector meson ρ are included in this description. The arrows in Eq. (1) indicate isovector quantities. The scalar self-interaction term $U(\sigma)$ of the σ meson is taken to be non-linear,

$$U(\sigma) = \frac{1}{2}m_\sigma^2\sigma^2 + \frac{1}{3}g_2\sigma^3 + \frac{1}{4}g_3\sigma^4. \tag{2}$$

The nucleon mass is M ; meson masses are m_σ , m_ω and m_ρ ; g_σ , g_ω and g_ρ are the corresponding coupling constants and $e^2/4\pi = 1/137$ is the fine structure constant. The field tensors for ω and ρ are given by $\Omega^{\mu\nu}$ and $\vec{R}^{\mu\nu}$; for the electromagnetic field it is $F^{\mu\nu}$. Recourse to the variational principle followed by the mean-field approximation treating the fields as c -numbers results in the Dirac equation for the nucleon and Klein-Gordon type equations for the mesons and the photon. For the static case, along with the time reversal invariance and charge conservation, the equations get simplified. The resulting equations known as the relativistic Hartree equation or RMF equation along with BCS approximation for inclusion of pairing are solved self-consistently to yield the fields and the single-particle states in an axially deformed basis expansion method [18].

The solution of the fields in the axially deformed basis for the odd-even or odd-odd nuclei is quite a difficult task. The time reversal symmetry in the mean field is violated for these systems. The odd particle induces polarisation current and time-odd component in the meson fields. The time-odd component plays important role in the description of magnetic moment and moment of inertia in rotating nuclei [19,20]. However, the effect on deformation and binding energies are very small and can be neglected to a good approximation [21]. In the present calculation for odd nuclei, we employ the blocking approximation [22] which restores the time reversal symmetry.

III. RESULTS AND DISCUSSIONS

For our calculation, we choose the NL3 parameter set [23] for the Lagrangian density given by Eq. (1). This particular set reproduces the bulk properties of nuclei quite satisfactorily including the nuclear matter incompressibility K_∞ . To check the sensitivity of the results with the choice of the parameter set we have also calculated the ground state properties of some of the isotopes near the drip line using NL1 and NLSH sets having significantly different K_∞ . Among these three sets, the results with the NL3 set are in better agreement with the experimental values. In the following we shall present the results calculated with the NL3 parameter set. The calculations have been performed by expanding fermionic and bosonic wave functions in 20 oscillator shells for axially deformed configuration. The $p - p$ and $n - n$ pairing correlations have been considered in the BCS approximation. The strength of these correlations are determined from the proton and neutron pairing gaps Δ_p and Δ_n evaluated from the experimental odd-even mass differences in the 4-point formula. The more accurate five-point formula [24] might have been employed, however, near the drip lines since some points would have been missed, for consistency we use the four-point formula throughout; moreover, the difference between the two is found to be very nominal. Though the experimental masses for the relevant nuclei are available [25] with large neutron excess, a few are still missing near the neutron drip line. The pairing gaps for these nuclei are taken by extrapolating the general trends of Δ_p and Δ_n .

A. Location of the F and Ne neutron drip

We have performed calculations for the binding energies of F and Ne isotopes extending from the stability line to the drip line lying around $N = 20$. In Fig. 1 the proton (filled circles joined by dashed line) and neutron (open circles joined by full line) pairing gaps for Ne and F are shown as a function of neutron number

as obtained from the 4-point formula. The circles are replaced by asterisks where the masses used are obtained from systematics [25]. The oscillations of Δ with maxima at even N and minima at odd N are manifestations of the weakening of pairing correlations for odd nucleon number [26]. It is seen that for F , there is a tendency of saturation for Δ_p and Δ_n at high values of N which is not that prominent for Ne isotopes. Beyond the experimentally available values, we take $\Delta_n = 1$ MeV for both the systems except for $N = 20$ where $\Delta_n = 0$ and for Δ_p we take 2 MeV and 3.5 MeV for Ne and F , respectively. The probable uncertainties for these choices may be ~ 0.5 MeV as can be estimated from Fig. 1.

The calculated ground state binding energies for the different isotopes of Ne and F along with the experimental binding energies are shown in Fig. 2. For both the systems it is seen that the agreement of the calculated values with the experimental ones are good upto $N = 16$ beyond which deviation starts building up. These deviations for F isotopes are larger by about a factor of 2 compared to those for Ne . It is difficult to gauge whether such large deviations can be explained in the relativistic Hartree-Bogoliubov (RHB) theory [8]. It may be mentioned that the agreement of the RMF binding energies with the experimental ones is very good even close to the neutron drip line for isotopes with atomic numbers $Z \geq 12$ [4]. This indicates that possibly the correlation effects beyond mean field play more important role for nuclei having neutron drip line around $N = 20$. However, since the uncertainties in the binding energy differences between two successive isotopes are much less, it is still meaningful to explore the drip-line characteristics for these nuclei.

In Fig. 3, we display the one-neutron separation energies S_n for the isotopes of Ne and F where the filled circles joined by the dashed line correspond to the experimental S_n [25] and the open circles joined by full line represent the calculated values with the NL3 parameter set. It is seen that the odd-even oscillations are similar to the observed ones for the two nuclei, however, there is some quantitative

disagreement, particularly for F with $N > 15$. The calculated two neutron separation energies S_{2n} for the two isotope chains are shown in Fig. 4 along with the available experimental values [25]. The stability of all the Ne isotopes agrees with the experimental findings, particularly, the stability of ^{29}Ne and the instability of ^{31}Ne . It may be pointed out that ^{29}Ne is found to be unstable in the shell-model calculation [5] contrary to the experimental finding. In our calculations, ^{29}F and ^{34}Ne lie on the drip line. The nucleus ^{31}F is found to be bound against one-neutron dripping but unbound by a few hundred KeV against two-neutron dripping contrary to the recent experimental observation [2] indicating that ^{31}F is a stable isotope. The pairing gaps were varied by 0.5 MeV but that does not change our conclusion. It may be pointed out that a very recent Monte-Carlo shell model (MCSM) calculation [15] also gets ^{31}F unbound by a few hundred KeV.

Recently, it has been pointed out [2] that the large deformation ($\beta_2 \sim 0.3$) is responsible for the extrastability of ^{31}F . To investigate the origin of the large deformation near the drip line, we display the evolution of the neutron and proton single particle energy levels in Figs. 5 and 6, respectively for the Ne and F nuclei around $N = 20$. The dashed lines in the figures correspond to the Fermi energies. From Fig.5 at $N = 20$, the gap between the $1d_{3/2}$ and $1f_{7/2}$ orbitals is ~ 6 MeV. With the increasing neutron number ($N > 20$) some of the m -components of these orbitals come very close to each other and thereby the lower m -components of the $1f_{7/2}$ orbital may behave like an intruder state; this induces large prolate deformation in both the systems. The proton orbitals do not show such behavior, this produces lower deformation for protons compared to that for neutrons near the drip line. The deformations for the F and Ne isotopes are displayed in Fig. 7 where these characteristics are evident.

The rms radii for protons and neutrons for the nuclei Ne and F as a function of neutron number are shown in Fig. 8. We note that the proton radius increases slowly with the neutron number, whereas the neutron radius follows approximately

an $N^{1/3}$ law. We find some undulations in the proton radii, particularly for the relatively lower neutron number. This may be traced back to the oscillations of the pairing gaps shown in Fig. 1. Higher the value of Δ , levels above the Fermi surface get higher occupancies producing larger radii. This is reflected in the radii shown in Fig. 8.

To study the effects of the different parameter sets on the location of the drip line nuclei, we repeated the calculations with the NL1 and the NLSH parameter sets. Though the absolute binding energies of different nuclei may vary by a few MeV depending on the parameter set, the conclusions regarding the drip line nuclei considered here remain unchanged.

B. Shell closure at N=16

A shell closure for nuclei gives rise to a break in the plot of one neutron separation energy (S_n) versus neutron number at fixed T_Z (i.e., neutron excess) [26]. Recent experimental data [10,27] available for the S_n clearly signals appearance of shell closure at $N=6, 16$ and 32 and disappearance of the conventional shell closure at $N=8$ and 20 for large values of T_Z . In this subsection, we mainly focus on the appearance of shell closure at $N = 16$. The calculated one-neutron separation energies S_n for odd- N and odd- Z nuclei for T_Z lying between 0 to 4 are displayed as a function of N in the upper panel of Fig. 9; its lower panel shows S_n for odd N and even Z nuclei with $1/2 \leq T_Z \leq 9/2$. The odd-even effects are eliminated with this choice. The magic number appears as a decrease of S_n with N [26]. The traditional magic number at $N=20$ is found to persist in our calculation for all T_Z (up to $T_Z = 9/2$) though experimentally there are indications of the dissolution of the magicity [10] at $N=20$ for $T_Z \geq 4$. At $N=16$, a clear break in S_n is seen for $T_Z \geq 3$ suggesting the appearance of a new shell closure at this neutron number. These correspond to the nuclei ^{23}N , ^{24}O , ^{25}F and ^{26}Ne . At $T_Z = 1$ corresponding to ^{30}Si a break in S_n is also observed; this does not correspond to a true shell

closure as discussed later.

In order to identify the shell closure more clearly, we also study the evolution of the deformation $|\beta_2|$ and the energy gap $\Delta\epsilon$ across the Fermi surface (the energy difference between the last occupied orbit and the first unoccupied one) with neutron number for different nuclei. In the upper panel of Fig. 10, the deformation of the isotopes of the odd- Z nuclei N , F and Na are shown; the same is displayed in the lower panel for the even- Z nuclei Ne , Mg and Si . All the isotopes of O considered are found to be spherical or nearly spherical; their deformations are not displayed here. For all the nuclei considered, the deformation vanishes at $N=20$ except for F having a minimum in $|\beta_2|$ with a small value. At $N=16$, the isotopes of N and Ne are found to be spherical reinforcing the existence of shell closure. For F , there is a local minimum in deformation at $N=16$ with a relatively small value of $|\beta_2| \sim 0.14$. Though there is an apparent break in S_n at $N=16$ for Si , no local minimum in β_2 is found at this neutron number. The deformations of Na and Mg at $N=16$ are relatively large.

The energy gap across the Fermi surface of a traditional closed-shell nucleus is relatively large compared to those of the neighbouring nuclei. In Fig. 11, the evolution of this gap $\Delta\epsilon$ for a few odd- Z (upper panel) and even- Z (lower panel) nuclei is displayed as a function of the neutron number. At $N=20$, all the nuclei that are stable show robust peaks. At $N=16$, the nuclei with $T_Z \geq 3$ also exhibit peaked structures. These peaks are relatively less prominent compared to those at $N=20$. From the examination of one neutron separation energy, deformation and shell gap, we observe an extra-stability for the nuclei with $N=16$ and with $T_Z \geq 3$; thus, the appearance of a new shell-closure at this N -value becomes evident. It is however weaker compared to the traditional one at the nearby neutron number $N=20$ for all T_Z considered here.

We have not included the effect of zero-point vibrations in our calculations, which in general influences the ground state energy. However, the parameters

of the effective Lagrangian have been determined through fitting the experimental ground state energies of some nuclei; further inclusion of zero-point oscillation may thus lead to some double-counting. The intrinsic state generated in the mean-field approximation is a superposition of states of different angular momenta; projection of the ground state of good angular momentum from this mixed state has in general an influence on both the ground state energy and the deformation. The angular momentum projection from the RMF state is a nontrivial task, we have not yet attempted it.

IV. SUMMARY AND CONCLUSIONS

We have calculated some recently observed ground state properties for the isotopic chains extending from the stability line to the neutron drip line for several light nuclei in the relativistic mean-field theory. It is found that though the binding energies of the isotopes near the drip line (around $N = 20$) are overestimated by a few MeV, the binding energy differences of neighbouring nuclei are fairly reproduced. The present calculation predicts ^{29}F and ^{34}Ne as drip line nuclei. Experimentally, till date ^{31}F is considered as the drip-line nucleus and for Ne upto mass number 32 has been observed. In our calculation, ^{31}F is bound against one neutron separation but unbound against two-neutron separation by only a few hundred KeV. The stability of ^{29}Ne and instability of ^{31}Ne found in our calculations are in agreement with the experimental observation.

The behaviour of the one neutron separation energy S_n , the deformation β_2 and the gap across the Fermi-surface of the neutron rich nuclei around $N=16$ clearly indicate the existence of a neutron shell closure at $N=16$ for $T_z \geq 3$. The dissolution of the neutron shell closure at $N=20$ for $T_z \geq 4$ suggested from experiments is however not observed in the present model.

The present calculation suffers from a number of limitations. The treatment of pairing in the BCS approximation is rather uncertain, particularly for the exotic

nuclei; the self-consistent Hartree- Bogoliubov approach for pairing is preferable. Correlations beyond the mean field may also be important in the present context. In a recent shell-model calculation [13], the mechanism for the appearance of shell-closure at $N=16$ and also the disappearance at $N=20$ for neutron-rich nuclei is attributed to the shift of the $1d_{3/2}$ level to higher energies closer to the $1f_{7/2}$ orbit. The microscopic origin of the reorganisation of the levels is claimed to lie in the spin-isospin part of the nucleon-nucleon interaction. In the present calculation, the level reorganisation is not that marked because of which the energy gap $\Delta\epsilon$ is not too large at $N=16$ and the shell-closure persists at $N=20$ even for very neutron-rich nuclei. The probable incompleteness of the present $\sigma - \omega - \rho$ version of the RMF theory for the description of very exotic systems is manifest here and is a possible pointer to the necessity of the inclusion of the pionic degrees of freedom in the RMF framework.

REFERENCES

- [1] H. Sakurai *et al*, Phys. Rev. C 54 (1996) R2802.
- [2] H. Sakurai *et al*, Phys. Lett. B 448 (1999) 180.
- [3] T. Motobayashi *et al*, Phys. Lett. B 346 (1995) 9.
- [4] G. A. Lalazissis, S. Raman and P. Ring, At. Data and Nucl. Data Tables 71 (1999) 1.
- [5] E. Caurier, F. Nowacki, A. Poves and J. Retamosa, Phys. Rev. C 58 (1998) 2033.
- [6] E. Caurier, F. Nowacki and A. Poves, Nucl. Phys. A 682 (2001) 1c.
- [7] Zhongzhou Ren, Z. Y. Zhu, Y. H. Cai and Gongou Xu, Phys. Lett. B 380 (1996) 241.
- [8] G. A. Lalazissis, D. Vretenar, P. Ring, M. Stoitsov and L. M. Robledo, Phys. Rev. C 60 (1999) 014310.
- [9] G. A. Lalazissis, D. Vretenar, W. Pöschl and P. Ring, Nucl. Phys. A 632 (1998) 363.
- [10] A. Ozawa, T. Kobayashi, T. Suzuki, K. Yoshida and I. Tanihata, Phys. Rev. Lett. 84 (2000) 5493.
- [11] H. Simon *et al*, Phys. Rev. Lett. 83 (1999) 496.
- [12] H. Keller *et al*, Z. Phys. A 348 (1994) 61.
- [13] T. Otsuka, R. Fujimoto, Y. Utsuno, B. A. Brown, M. Honma and T. Mizusaki, Phys. Rev. Lett. 87 (2001) 082502.
- [14] E. K. Warburton, J. A. Becker and B. A. Brown, Phys. Rev. C 41 (1990) 1147.

[15] Yutaka Utsuno, Takaharu Otsuka, Takahiro Mizusaki and Michio Honma, Phys. Rev. C 64 (2001) 011301(R).

[16] Y. K. Gambhir, P. Ring and A. Thimet, Ann. Phys. (N. Y.) 198 (1990) 132.

[17] B. K. Agrawal, Tapas Sil, S. K. Samaddar and J. N. De, Phys. Rev. C 62 (2000) 044307.

[18] P. Ring, Y. K. Gambhir and G. A. Lalazissis, Comput. Phys. Commun. 105 (1997) 77.

[19] U. Hoffmann and P. Ring, Phys. Lett. B 214 (1988) 307.

[20] A. Afanasjev, J. König and P. Ring, Nucl. Phys. A 608 (1996) 107.

[21] G. A. Lalazissis, D. Vretenar and P. Ring, Nucl. Phys. A 650 (1999) 133.

[22] S. K. Patra, M. Del Estal, M. Centelles and X. Viñas, Phys. Rev. C 63 (2001) 024311.

[23] G. A. Lalazissis, J. König and P. Ring, Phys. Rev. C 55 (1997) 540.

[24] M. Bender, K. Rutz, P. G. Reinhard and J. A. Maruhn, Euro. Phys. Jour. A 8 (2000) 59.

[25] G. Audi, O. Bersillon, J. Blachot and A. H. Wapstra, Nucl. Phys. A 624 (1997) 1.

[26] A. Bohr and B. Mottelson, Nuclear Structure , Vol. II (W. A. Benjamin, New York 1969), Ch. 2.

[27] R. Kanungo, I. Tanihata and A. Ozawa, RIKEN-AF-NP-401, (2001).

Figure Captions

Fig. 1 Experimental pairing gaps for neutron (open circles joined by full line) and proton (filled circles joined by dashed line) for the isotopes of Ne (top panel) and F (bottom panel). The asterisks stand for results obtained using masses from systematics.

Fig. 2 Calculated (with the NL3 parameter set) and experimental binding energies for different isotopes of Ne (top panel) and F (bottom panel). The asterisks stand for results obtained using masses from systematics.

Fig. 3 Calculated (open circles joined by full line) and experimental (filled circles joined by dashed line) one-neutron separation energies S_n for the different isotopes of Ne (top panel) and F (bottom panel). Calculations are performed with the NL3 parameter set. The asterisks stand for results obtained using masses from systematics.

Fig. 4 Same as in Fig. 3 for two-neutron separation energies S_{2n} .

Fig. 5 Neutron single-particle spectra around the Fermi surface (dashed line) for different isotopes of Ne (top panel) and F (bottom panel) close to the drip line calculated with the NL3 parameter set.

Fig. 6 Same as in Fig. 6 for the proton spectra.

Fig. 7 Neutron quadrupole deformation $\beta_2(n)$ (dashed line) and proton quadrupole deformation $\beta_2(p)$ (dotted line) for the different isotopes of Ne (top panel) and F (bottom panel) calculated with the NL3 parameter set. The open circles joined by full line represent the total deformation.

Fig. 8 Neutron (open circles joined by full line) and proton (filled circles joined by dashed line) rms radii for the different isotopes of Ne (top panel) and F (bottom panel) calculated with the NL3 parameter set. The arrows on the

abscissa correspond to the locations of the neutron drip lines obtained in the present calculation. The asterisk symbols refer to the experimental proton rms radii. In the upper panel, the open and filled squares joined by full and dashed lines, respectively, refer to the neutron and proton rms radii from Ref.[9].

Fig. 9 One neutron separation energy (S_n) as a function of neutron number for odd-odd (upper panel) and odd-even (lower panel) nuclei.

Fig. 10 The magnitude of the ground state deformation $|\beta_2|$ as a function of neutron number for a few odd-Z (upper panel) and even-Z (lower panel) nuclei.

Fig. 11 The same as in Fig. 10 for the energy gap $\Delta\epsilon$ across the Fermi surface.

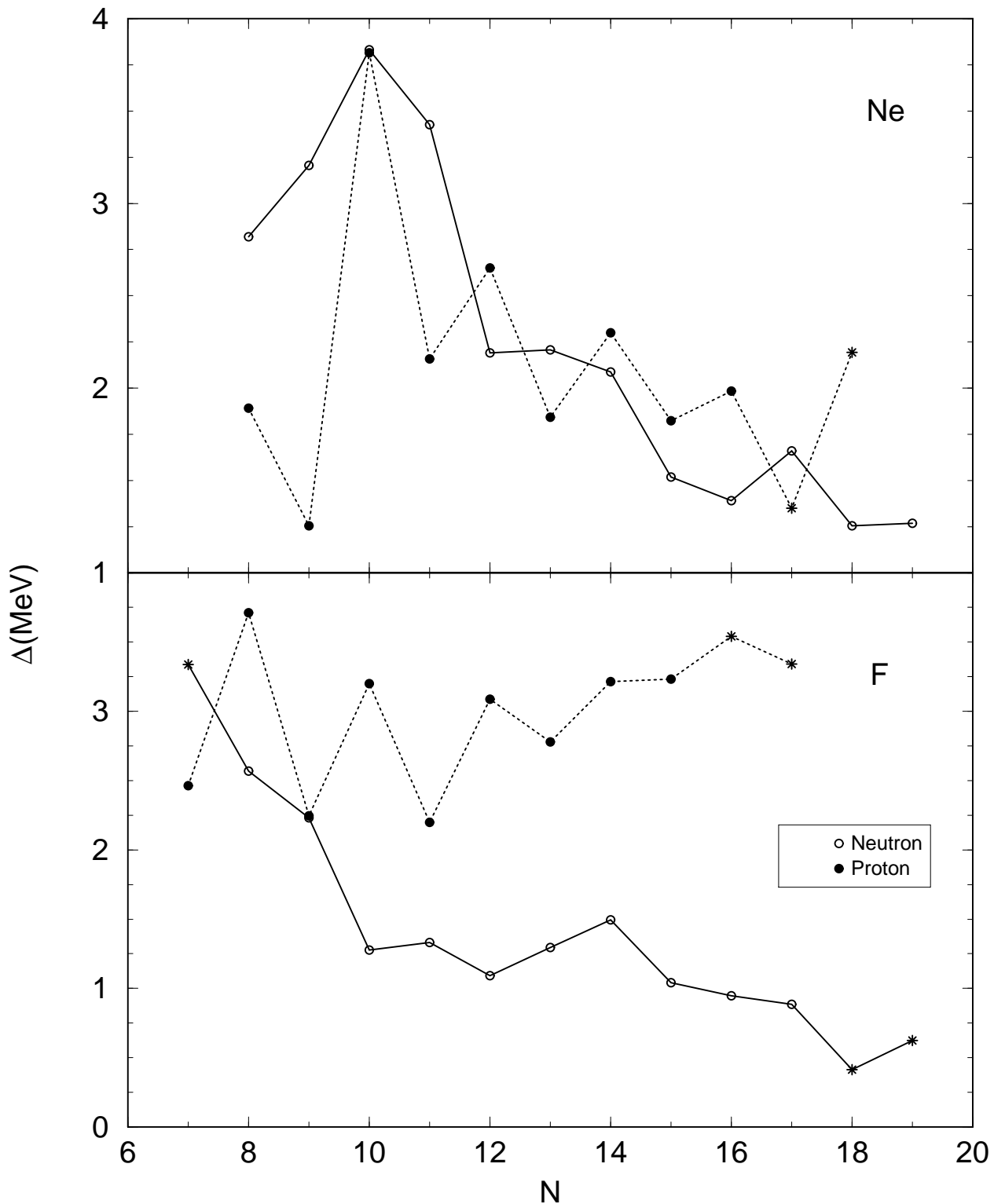


Fig. 1

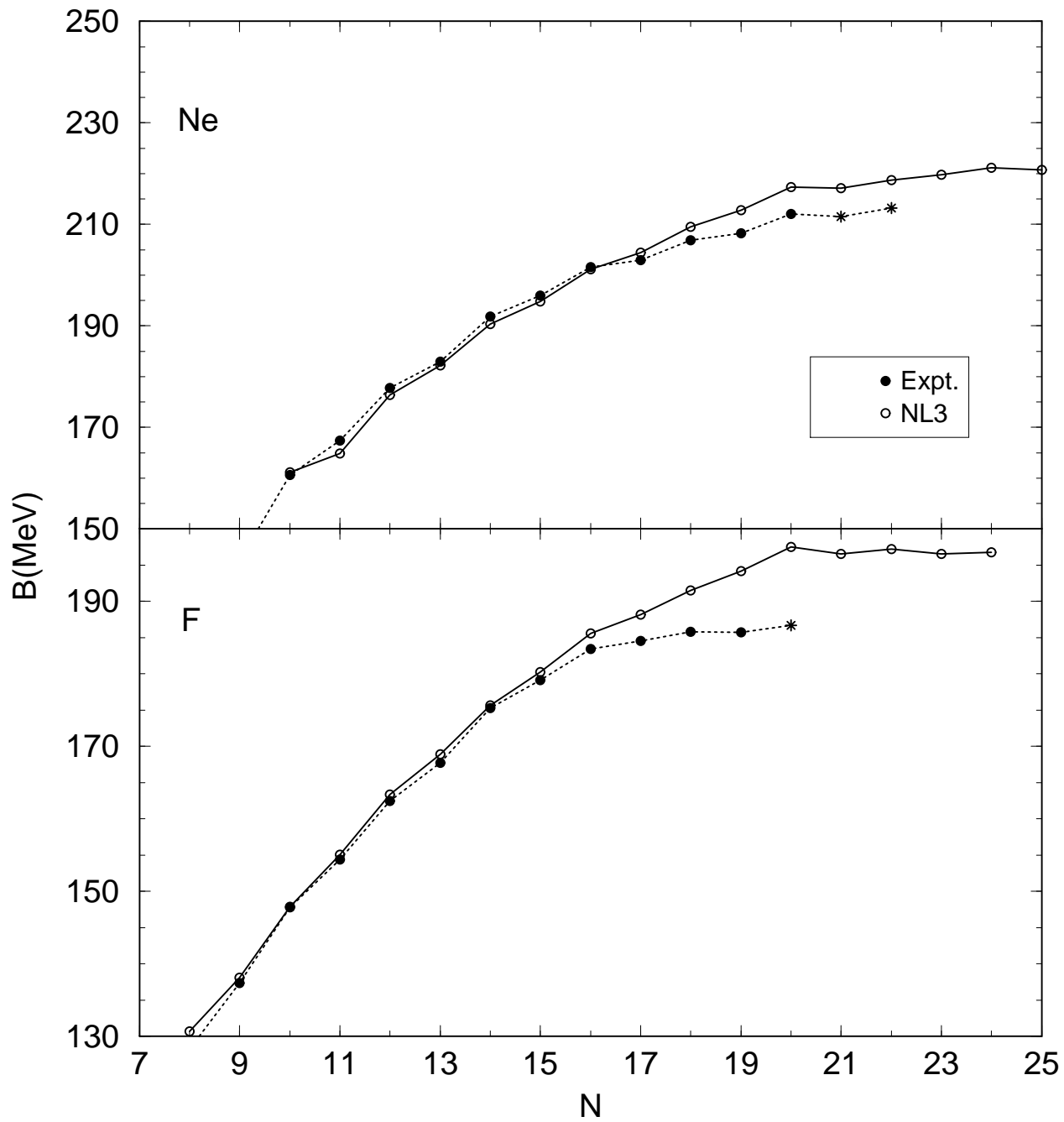


Fig. 2

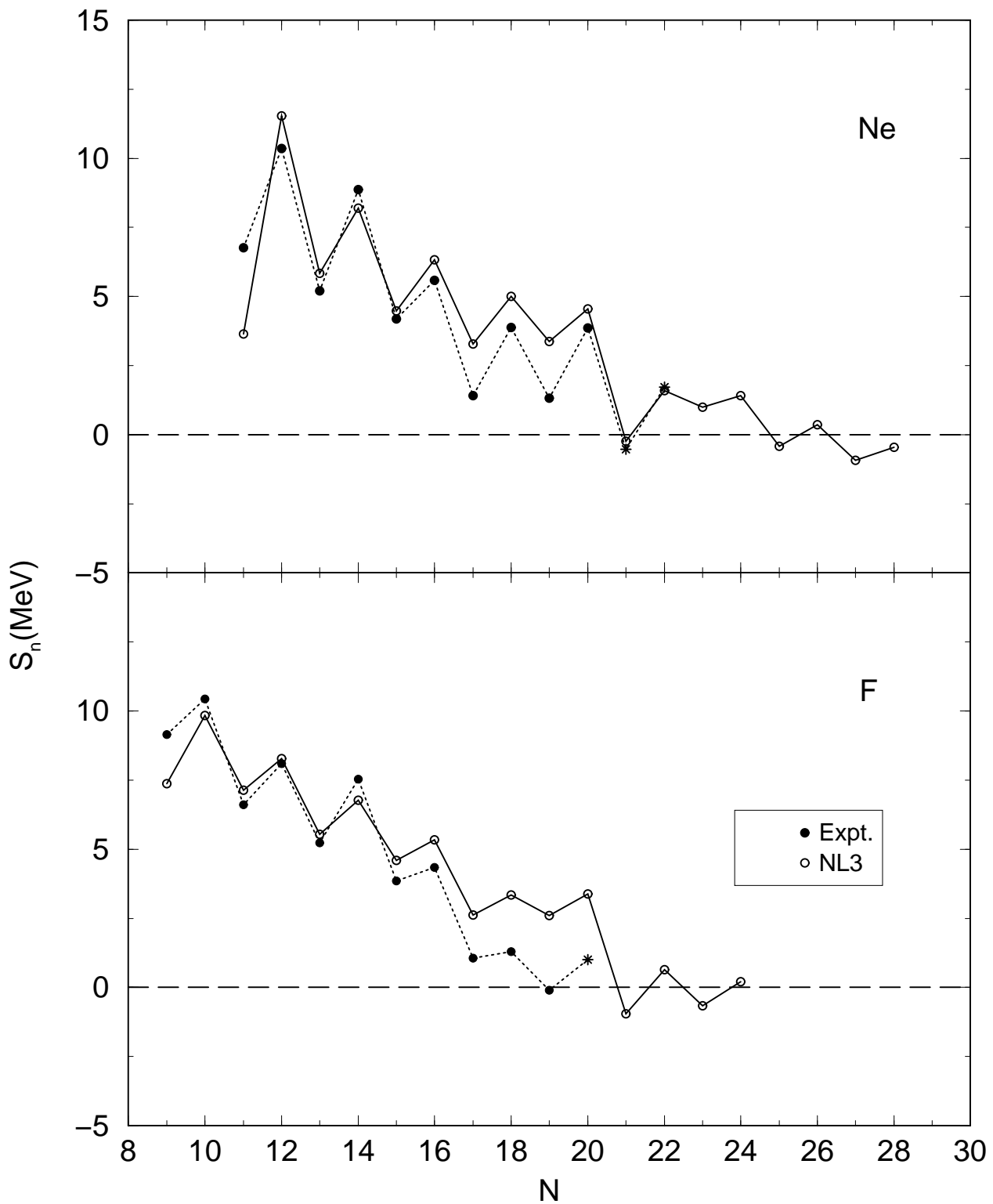


Fig. 3

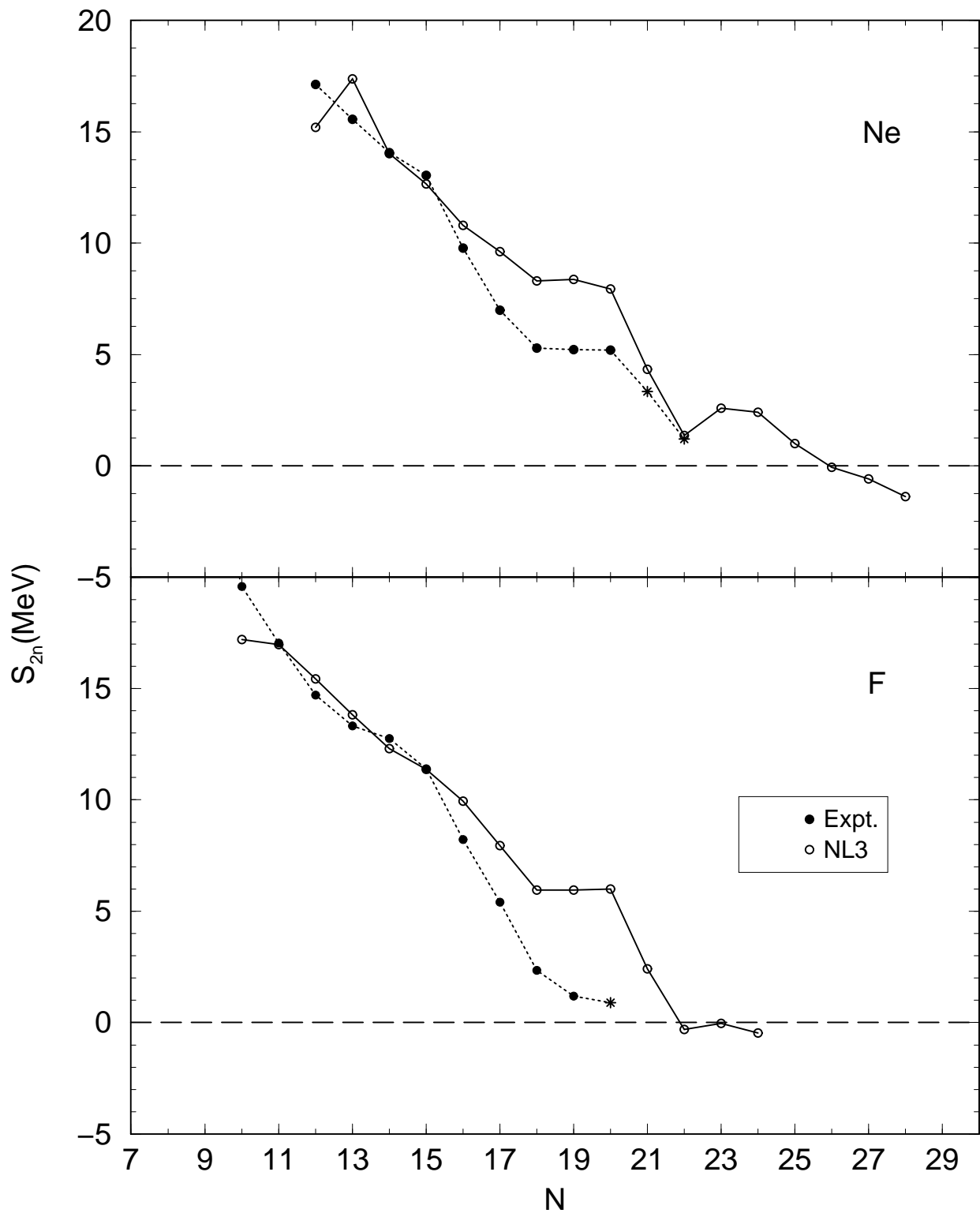


Fig. 4

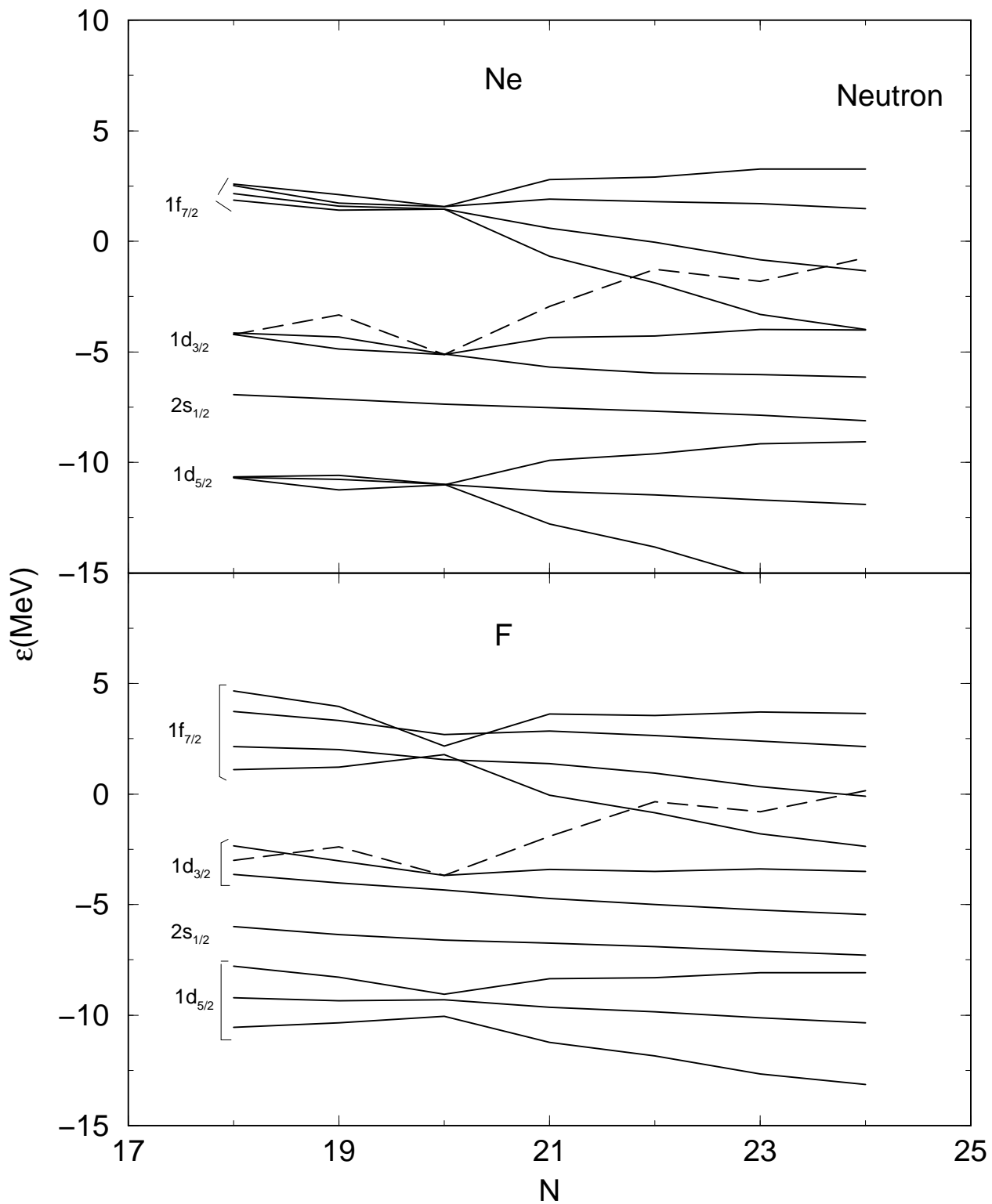


Fig. 5

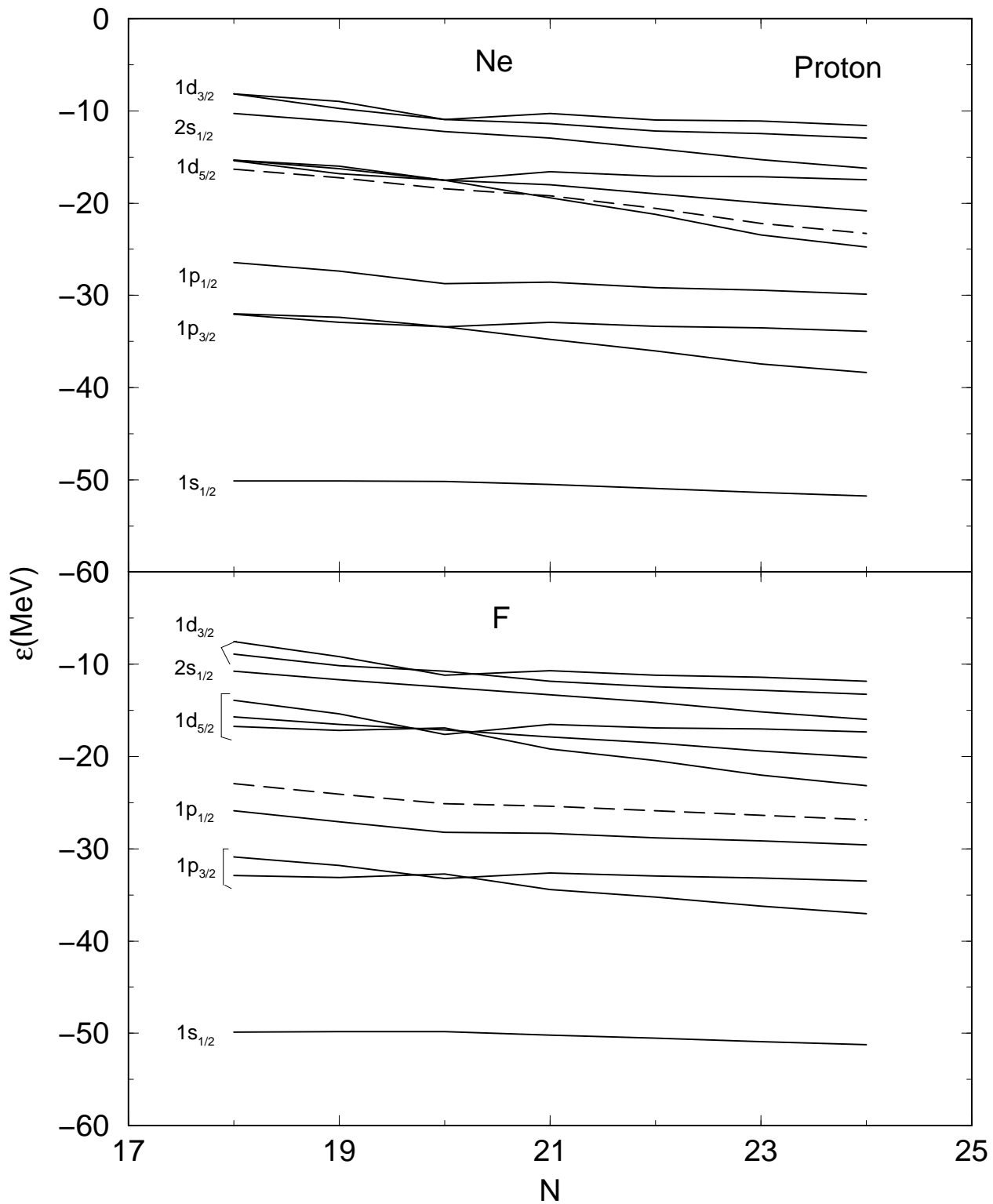


Fig. 6

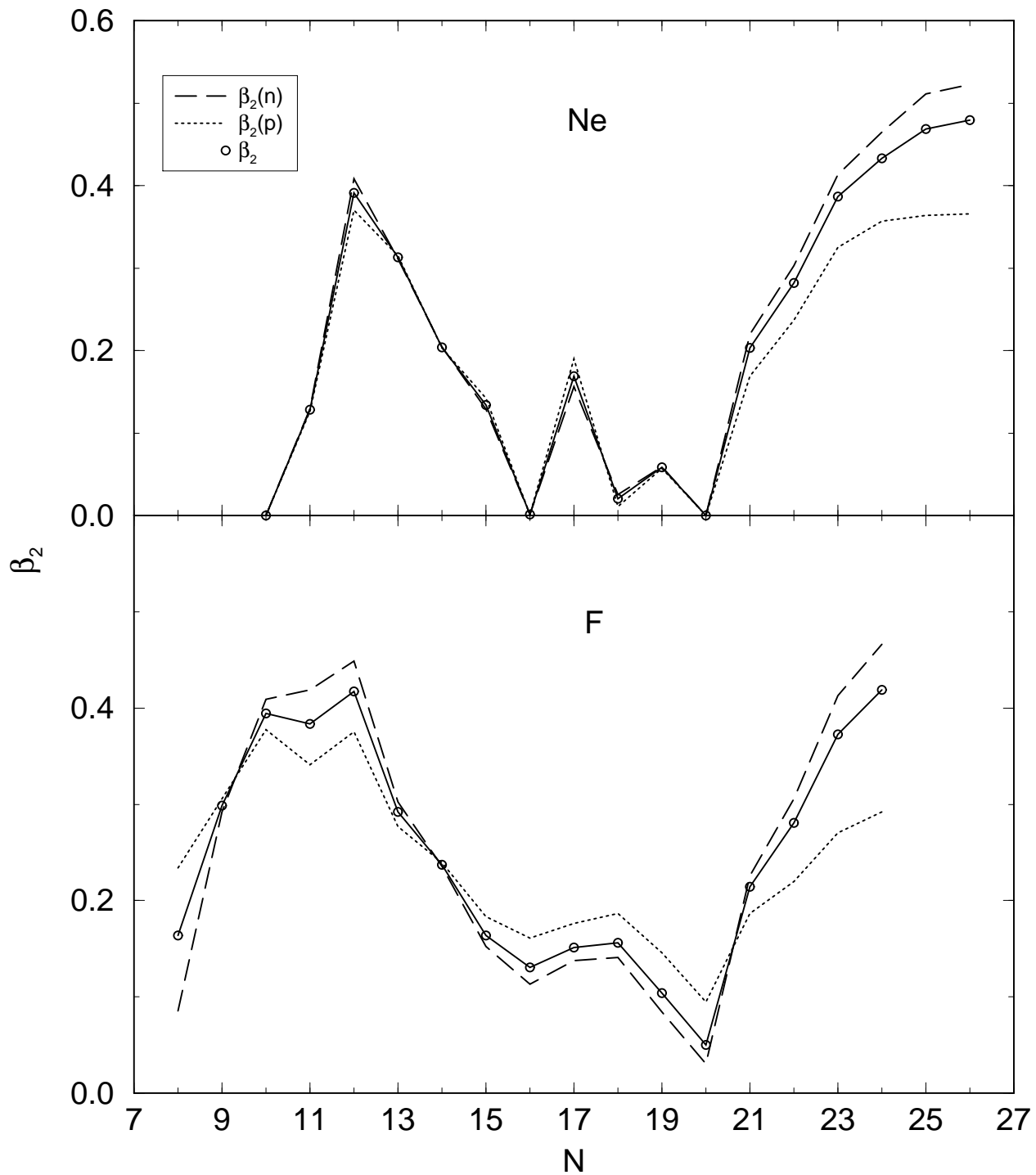


Fig. 7

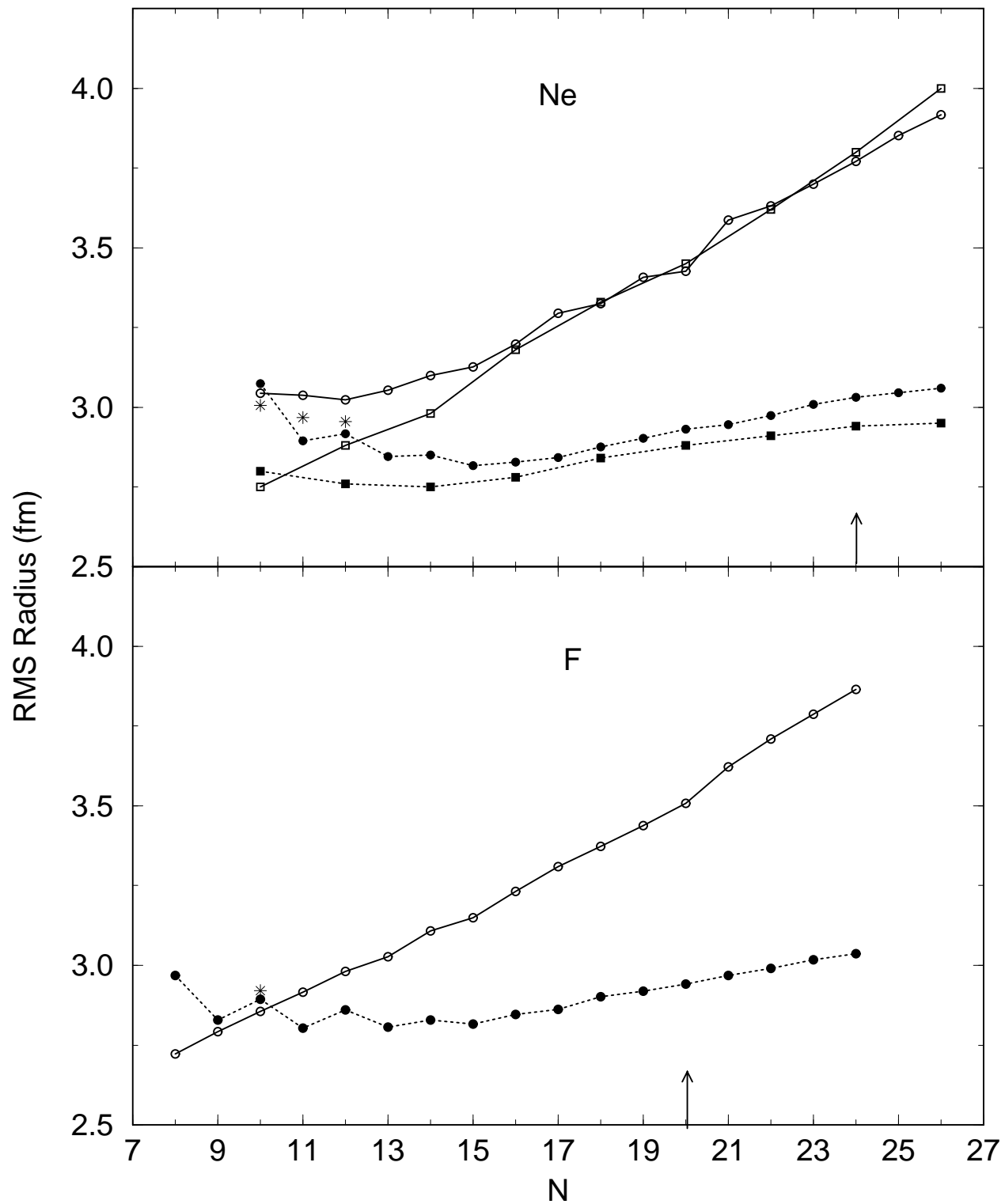


Fig. 8

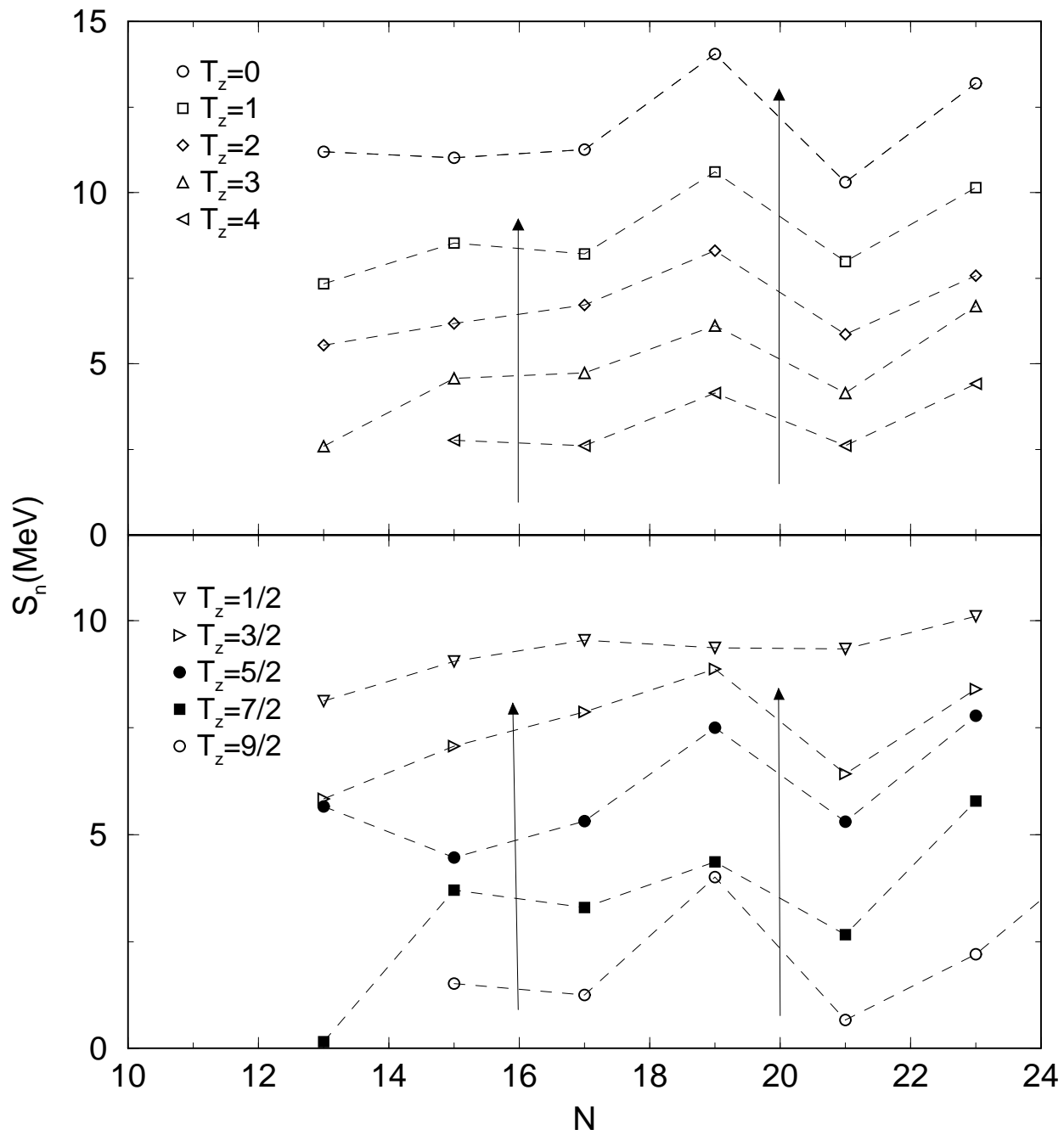


Fig. 9

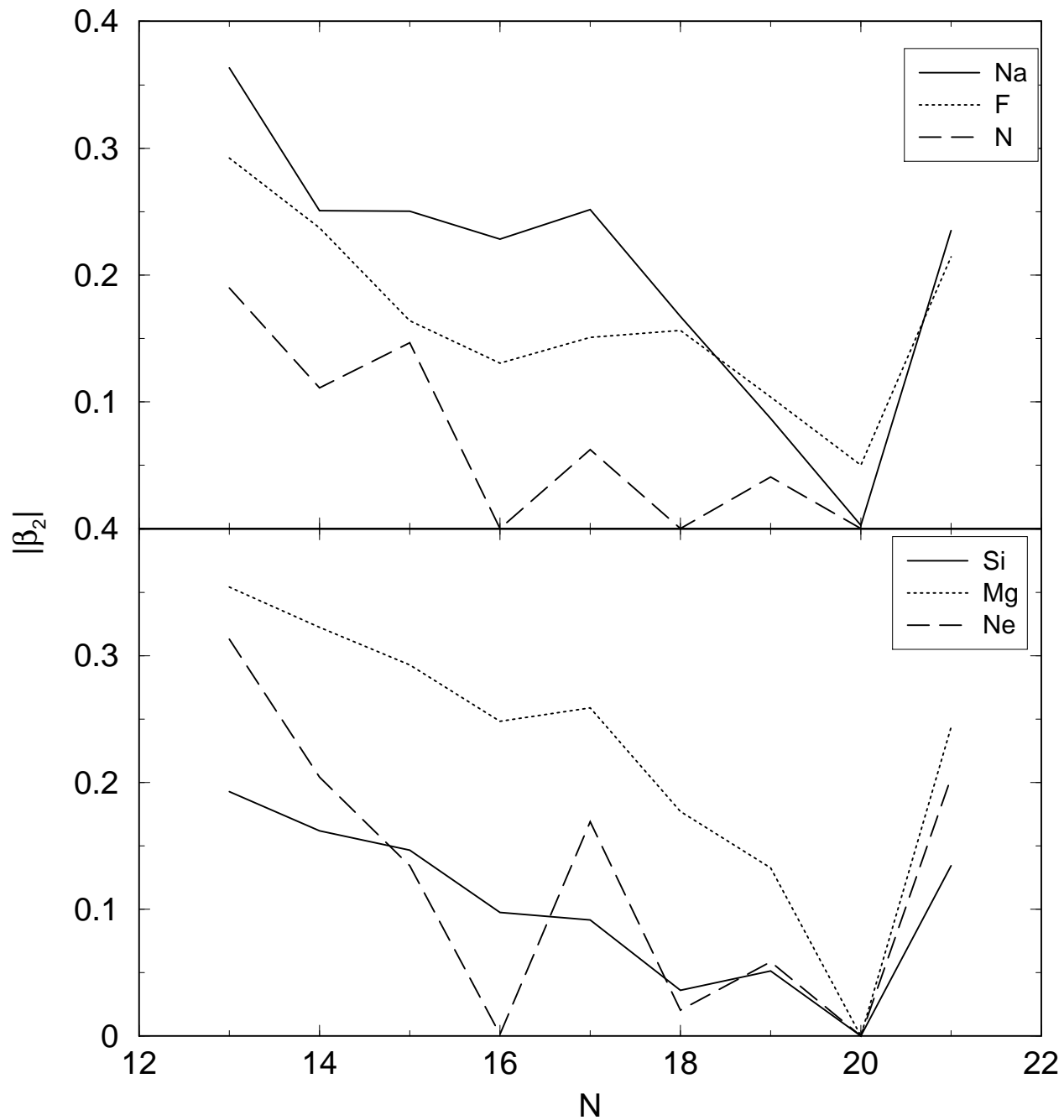


Fig. 10

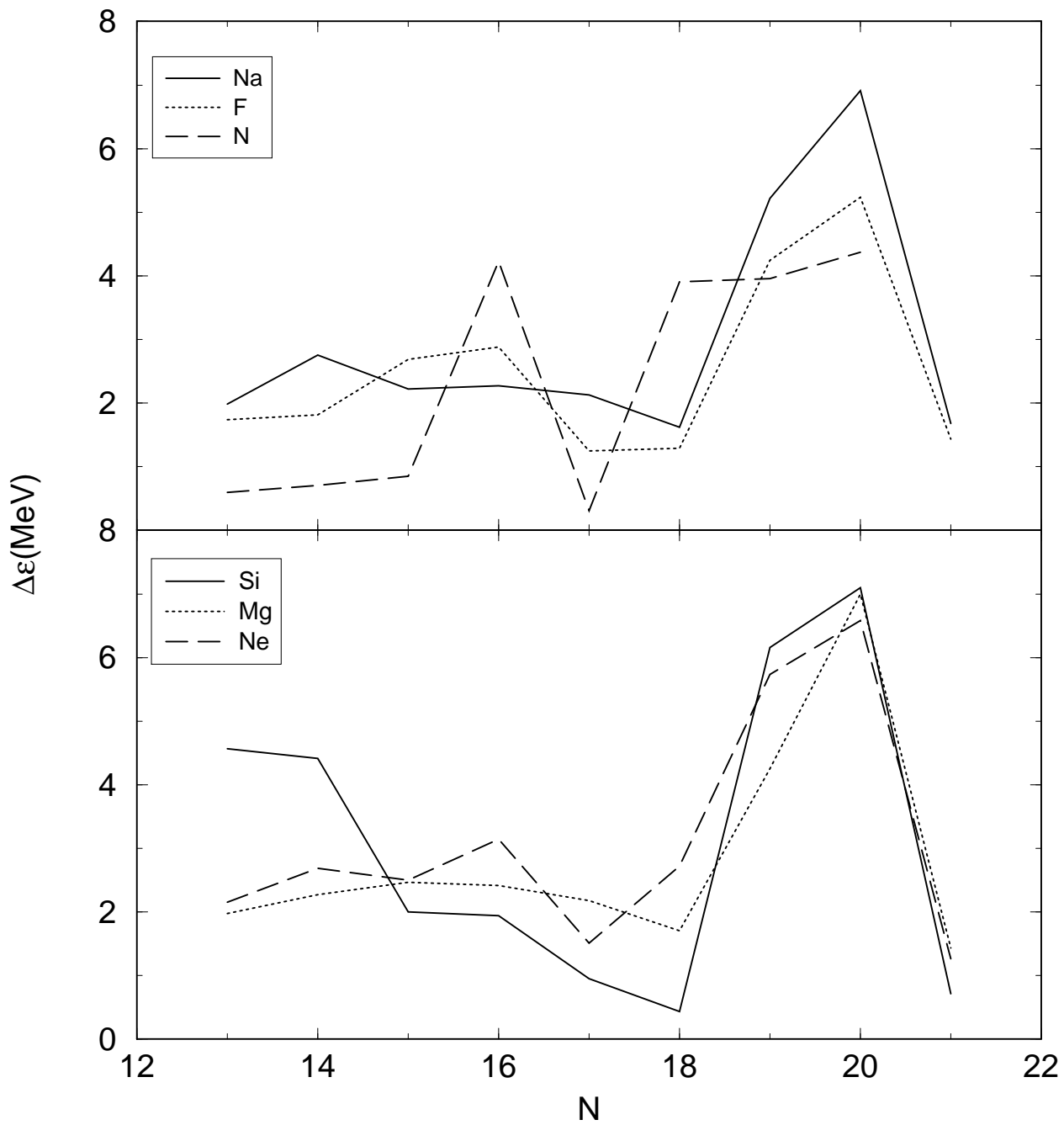


Fig. 11